HAL
open science

Surface treatment methods for mitigation of hydrothermal ageing of zirconia

Chong Wei, Laurent Gremillard

To cite this version:

Chong Wei, Laurent Gremillard. Surface treatment methods for mitigation of hydrothermal ageing of zirconia. Journal of the European Ceramic Society, 2019, 39 (14), pp.4322-4329. 10.1016/j.jeurceramsoc.2019.06.013 . hal-02156270

HAL Id: hal-02156270

https://hal.science/hal-02156270v1

Submitted on 14 Jun 2019

HAL is a multi-disciplinary open access archive for the deposit and dissemination of scientific research documents, whether they are published or not. The documents may come from teaching and research institutions in France or abroad, or from public or private research centers.

L'archive ouverte pluridisciplinaire **HAL**, est destinée au dépôt et à la diffusion de documents scientifiques de niveau recherche, publiés ou non, émanant des établissements d'enseignement et de recherche français ou étrangers, des laboratoires publics ou privés.

Surface treatment methods for mitigation of hydrothermal ageing of zirconia

Published in: Journal of the European Ceramic Society, 2019

https://doi.org/10.1016/j.jeurceramsoc.2019.06.013

Chong WEI[1,2], Laurent GREMILLARD[2,+]

[1] School of Mechanics, Civil Engineering and Architecture, Northwestern Polytechnical University, Xi'an 710072, P. R. China

[2] Univ Lyon, INSA-Lyon, CNRS, MATEIS UMR5510, F-69621 Villeurbanne, France

[+] Corresponding author

Abstract

Hydrothermal ageing of zirconia ceramics (tetragonal-to monoclinic phase transformation in the presence of humidity) is highly sensitive to the surface characteristics. Thus chemical modifications of the surfaces over a few microns may be a good way to mitigate ageing without affecting bulk mechanical properties. Here, the efficiency of different post-sintering thermal treatments in powder beds of different compositions to prevent or slow down hydrothermal ageing of 3Y-TZP is tested. The microstructure, ageing kinetics at different temperatures and mechanical properties of the treated samples are then evaluated.

Treatments with 12Ce-TZP proved to be the most efficient to limit ageing at 134°C while keeping good mechanical properties. However, this is accompanied by a decrease of the activation energy of ageing, thus by an acceleration of ageing at lower temperature. These results also show that the activation energy of ageing is material-dependant, thus should be ascertained for every developed zirconia-based ceramic.

Keywords

Zirconia; hydrothermal ageing; surface treatments

Introduction

Zirconia ceramics are well known for their tetragonal-to-monoclinic phase transformation, responsible for their excellent mechanical properties when it occurs around a propagating crack [1]. However, when it occurs on the surface of zirconia pieces in the presence of water vapour, the t-m phase transformation gives rise to hydrothermal ageing, also called Low Temperature Degradation (LTD) [2-4]. Since it begins on surfaces, hydrothermal ageing is particularly sensitive to surface characteristics. Thus how to get a superior anti-ageing surface without sacrificing the excellent mechanical properties of zirconia becomes a hot topic for improving zirconia lifetime. Numerous studies have been conducted along these axes, with various success. For example, Chevalier et al. studied zirconia dental implants coated with a porous zirconia layer (aimed at better osseointegration), but showed that the porous coating accelerated hydrothermal ageing [5]. Oblak et al. found that the initial strength and survival rate of a dental Y-TZP ceramic material to fatigue testing was highly dependent upon surface preparation: in particular ground samples and sandblasted samples (especially sandblasted ones) have better resistance to LTD than as-sintered samples [6]. Deville et al. studied the effects of surface finish on ageing kinetics of biomedical grade zirconia and pointed out that rough polishing was beneficial for ageing resistance [7]. Inokoshi et al. found that surface treatments (rough polishing, sandblasting with Al_2O_3, tribochemical silica sandblasting) improved the ageing resistance of Y-TZP zirconia, decreased the ageing resistance of Y-TZP/Al_2O_3 composite, and did not affect the LTD behavior of Ce-TZP/Al_2O_3 composites. Pozzobon et al. pointed out that the tribochemical treatment (sandblasting treatment) and silica nano-film deposition did not reduce mechanical properties of Y-TZP ceramic [8]. Camposilvan et al. proposed a cerium-containing anti-ageing surface, formed during sintering after impregnating porous pre-sintered zirconia samples with a cerium-containing solution [9].

In this work we examine the efficiency of different surface treatments of zirconia, consisting in a post-sintering heat treatment of fully dense materials on powder beds of different compositions with the aim of enriching the surface in stabilizing elements (Y or Ce). The ageing behaviour and some mechanical properties are tested on the surface-modified samples.

Materials and methods

Materials processing

The samples were commercial 3Y-TZP polished disc (Doceram, Germany), with 20 mm diameter and 1 mm height, sintered at 1500°C. The samples were heat-treated (post-sintering treatment) on powder beds made of Y-TZP powders with 3 or 8 mol.% Y_2O_3 as a stabilizer (TZ3YE or TZ8YS produced by Tosoh), or of zirconia stabilized with 12 mol.% CeO_2 (12Ce-TZP powder: CeZ12, Daiichi).

During post-sintering treatment, the samples were completely embedded inside the powder beds (at least 2 mm thick on each side), then two thermal treatments were tested: the first one consisted in heating to 1490°C (thus below the sintering temperature of the samples) for 0.3 h at 5°C/min, cooling down to 1350°C for 1 h at 200°C/min, and finally cooling down to room temperature at 5°C/min; the second thermal treatment was applied only to the treatments with 12Ce-TZP, and consisted in heating to 1550°C (above the sintering temperature of the samples) for 0.5 h at 5°C/min, and cooling down to room temperature at 5°C/min. 7 samples were prepared for each condition. Note that in order to observe properly the grain size and Yttria content in control samples, one control sample was submitted to a thermal etching (1250°C, 30 min) that also allowed the removal of machining residual stresses.

The samples prepared during this study are summarized in Table 1. Throughout the paper they will be referred to as (CS)-(Powder)-(Post Sintering temperature): for example, CS-3Y-1490 refers to the samples treated at 1490°C on a TZ3YE powder bed (CS stands for Commercial Sample).

Two types of control samples were also used. The ones referred to as "Control" are as-received material, without further preparation. The ones referred to as "Control+TT1250" were polished then annealed at 1250°C (30 min) to remove residual stresses and reveal grain boundaries in order to allow the characterization of the bulk properties of the starting material.

The particle size distributions of the powders used for the powder beds were measured using laser granulometry (Malver Mastersizer 2000).

Table 1 : Sample preparation summary. X is powder name (3Y, 8Y, 12Ce…)

Sample name	original sample	post sintering condition	Powder	ageing temperature/°C	Number of samples
Control	Commercial samples	no treatment		90, 100, 111, 121, 134	7
Control + TT1250	Commercial samples	Polishing, 1250°C 0.5h			1
CS-X-1490	Commercial samples	T1 1490°C-0.3h, T2 1350°C-1h	3Y-TZP, 8Y-TZP, 12Ce-TZP	90, 100, 111, 121, 134	7 per powder
CS-12Ce-1550	Commercial samples	1550°C-0.5h	12Ce-TZP	90, 100, 111, 121, 134	7

Microstructural analyses: proportion of cubic phase, yttria content

Scanning Electron Microscopy (SEM) observations were conducted using a Zeiss Supra55 VP microscope, in vacuum, using a low voltage (2 kV) without conductive coating. Grain size was calculated from SEM observations, using the linear intercept method (using around 20 lines on at least 5 pictures). Energy dispersive X-Ray spectroscopy (EDS) analyses were conducted in the same SEM operated at 25 kV acceleration voltage, with an Oxford Silicon Drift Detector (SDD). For each sample 5 spectra were recorded on large areas on the surface (~1.3x1.8 mm² or ~170x220 µm²) to evaluate the surface concentration in Ce, Zr and Y (in these conditions, depth analysed by EDS is around 1.5µm). On sample CS-12Ce-1550, EDS line scans were also performed on polished cross section using the same experimental conditions, to evaluate the diffusion depth of Ce.

When possible, the average Y_2O_3 content in tetragonal phase was obtained from X-ray diffraction (XRD) data, using a procedure detailed in ref [10]. To summarize, first a calibration curve of the amount of Y_2O_3 in the cubic and tetragonal phases *versus* the lattice parameters was established, from PDF files and previous work by Scott [11-13]. Then XRD patterns were recorded over a large angular range (15-120 deg. 2θ) and analysed using an iterative procedure based on Rietveld refinement (with Topas 4.0 software (Bruker, Germany)), to obtain the proportions of the different phases (cubic and tetragonal), the lattice parameters of the tetragonal phase (in most materials cubic peaks were lost in the background

or convoluted with some tetragonal peaks) and finally the amount of yttria in the tetragonal phase with the help of the calibration curve.

Hardness analysis and crack propagation threshold

The hardness was measured by using a Vickers hardness tester (Future-tech Testwell HV700) with a 20 kg load and a 10 s dwell time (20 indents distributed over 5 samples). The threshold for crack propagation (K_{I0}) was evaluated from the radial crack pattern accompanying the same 20 Vickers indentations (measured at least 72 hours after indentation so that the radial cracks reached a stable shape and length) and calculated according to Anstis' equation [14]. As zirconia is sensitive to subcritical crack propagation, under the influences of the humidity present in atmosphere and of the residual stresses around the Vickers indent the cracks can propagate until the K_I reaches the threshold value K_{I0}. In these conditions Anstis' equation does not give access to K_{Ic}, but to K_{I0} [15, 16].

Statistical analyses of K_{I0} and Hv were conducted in GraphPad Prism version 7.03 (GraphPad Software) with $p \leq 0.05$ considered statistically different. Normality was checked with the Kolmogorov-Smirnov test and equal variance assumption was tested with the Bartlett test. Since the normality but not the equal variance assumption was satisfied for K_{I0}, a non-parametric Kruskal-Wallis test was conducted, with Dunn's post-hoc and $p \leq 0.05$ considered statistically different. Since H_v data passed both normality and equal variance tests, a One-Way ANOVA was conducted for this dataset, with Tukey's post-hoc and $p \leq 0.05$ considered statistically different. Data are represented as notched box plots with minimum, lower quartile, median, upper quartile and maximum for each group (n=20 per group).

Assessment of ageing kinetics

Ageing kinetics was evaluated by performing accelerated ageing tests on all samples in water steam at 134 ◦C, under 2 bars pressure.

The amount of tetragonal to monoclinic phase transformation was measured by X-ray diffraction. XRD patterns were recorded in the 27-33° (2θ) range with a scan speed of 0.2 $°\cdot s^{-1}$ and a step size of 0.05°. The monoclinic ZrO_2 phase content (V_m) [17] was calculated by:

$$V_m = \frac{1.311X_m}{1+0.311X_m} \qquad \text{Eq. 1}$$

The value of X_m[18] being calculated as:

$$X_m = \frac{I_m^{-111}+I_m^{111}}{I_m^{-111}+I_m^{111}+I_t^{101}} \qquad \text{Eq. 2}$$

Where I_p^{hkl} is the area of the diffraction peak related to the (hkl) plane of phase p (m for monoclinic and t for tetragonal).

The hydrothermal ageing kinetics are rationalized by fitting the transformation curves with the Mehl–Avrami–Johnson laws[19]:

$$f = \frac{V_m-V_0}{V_{max}-V_0} = 1-\exp(-(bt)^n)\,,\ b = b_0\exp\left(-\frac{Q}{RT}\right) \qquad \text{Eq. 3}$$

where f is the degree of advancement of the transformation, V_m is the monoclinic phase content, V_{max} and V_0 are respectively the saturation and initial levels of monoclinic phase content, n is an exponent that depends on both nucleation and growth kinetics of the monoclinic phase [20] and b is a thermally activated parameter (with Q the activation energy, R the gas constant, and T the absolute temperature).

To measure Q, on each material ageing kinetics were measured at 90, 100, 111, 121 and 134°C at 100% relative humidity in autoclave (Wolf Sanoclav LA-MCS; one sample by temperature). Then all kinetics were analysed using Eq. 3. The parameters V_{max}, b_0 and Q for a given material were determined by minimising the sum of the absolute differences between the calculated and experimental points (using Microsoft Excel solver with Non Linear GRG algorithm).

Results

Powder bed characterization

Figure 1 shows the particle size distribution of the three powders used for the powder bed. The measurement were performed on dry powders, thus are representative of the agglomeration state inside the powder beds. All powders were spray dried by the producer. The 8Y-TZP powder is monodisperse with d50 around 34µm. 3Y-TZP and 12Ce-TZP present a few big agglomerates, and 2 other populations: granules around 10 µm diameter and particles around 0.6 µm. This is coherent with the particle size given by the producer of CeZ12, but hints to a limited aggregation of 3Y-TZP particles since in TZ3Y-E the individual particle size should be around 40 nm (as claimed by the producer).

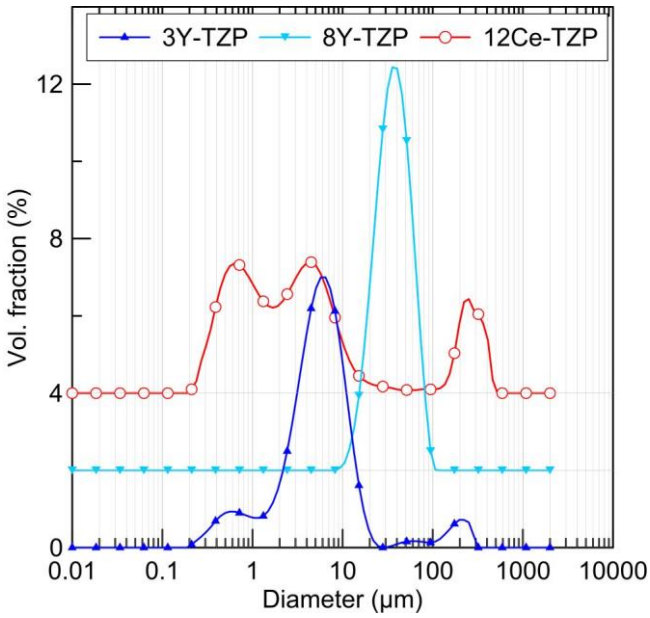

Figure 1: particle size distributions of the powder beds

Microstructural analyses

Figure 2 shows that there were no significant differences between the surfaces of CS-3Y-1490 and CS-8Y-1490. Large-sized grains appeared on the surface of CS-12Ce-1490. The highest post-sintering temperature used for CS-12Ce-1550 led to larger grains on the surface. The phase content and phase partitioning were analysed by X-ray diffraction (Figure 3) coupled to Rietveld analysis. The results of these microstructural analyses are shown in Table 2. Essentially, no microstructural changes were detected when using 3Y-TZP or 8Y-TZP as a powder bed. On the other hand, CS-12Ce-1490 and CS-12Ce-1550 exhibited higher amount of cubic phase on the samples surfaces. Finally a secondary tetragonal phase was found on

CS-12Ce-1550 sample (arrow on Figure 3), and attributed to Ce-doped tetragonal grains on the surface (with depth much lower than 5µm, the analysed depth with the XRD configuration used here). Unfortunately, no calibration curve could be established to determine the Y and Ce content in Y-Ce-TZP from the lattice parameters. Thus the stabilizers contents in CS-12Ce- samples cannot be known from XRD measurements.

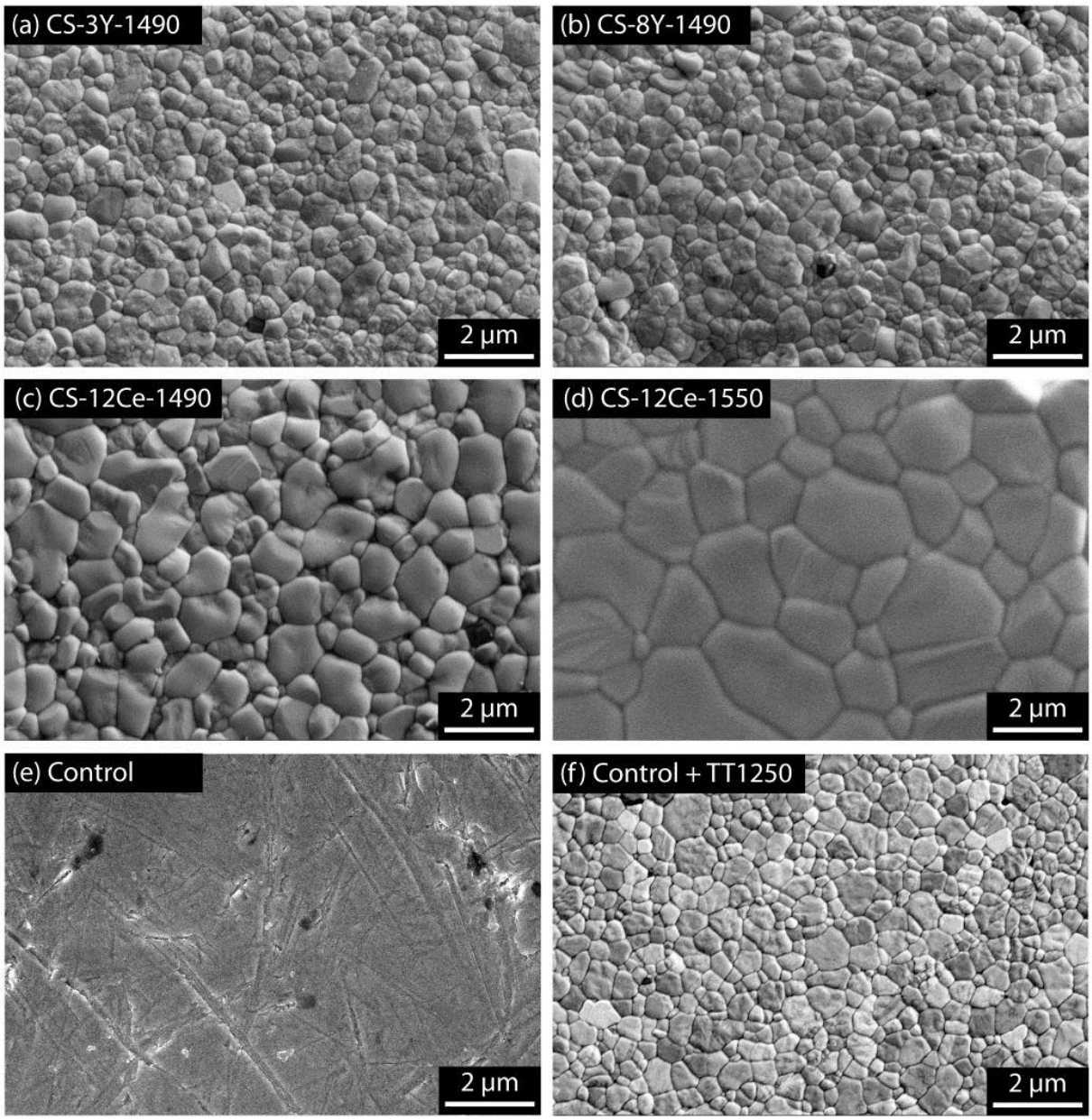

Figure 2 : SEM micrographs of samples after post sintering

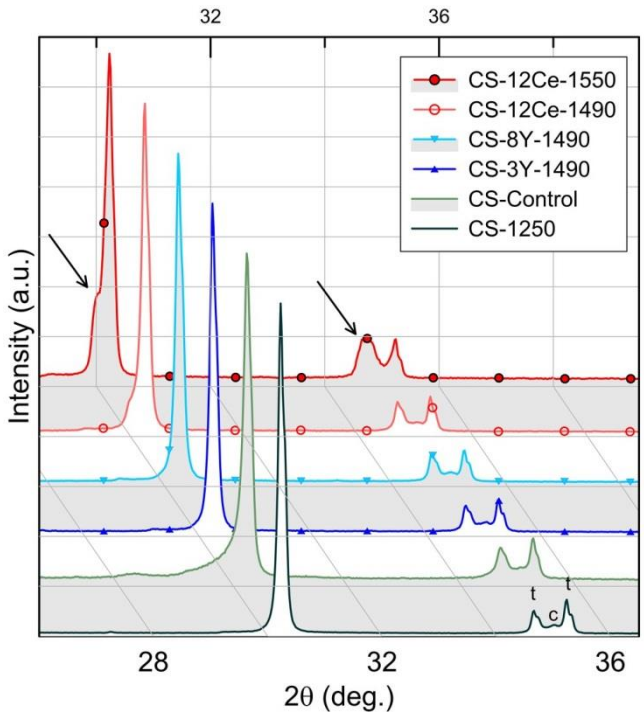

Figure 3: X ray diffraction diagrams of CS materials. The arrow points to peaks that can be attributed to the presence of a secondary (Ce-doped) tetragonal phase. t and c respectively refer to tetragonal and cubic phases.

In the conditions used here, the spatial resolution (in X, Y and Z) of EDS analysis can be estimated at around 1.5 µm [21]. EDS analyses show that the overall yttrium content did not change with post-sintering treatment, whatever the powder bed (in spite of the slight evolutions reported in Table 2, t-test show no statistically significant difference). However, a clear evolution of the surface Ce content was observed for samples treated on 12Ce-TZP beds (Ce/Zr molar ratio (average on the first 1.5µm) from 2 mol.% for CS-12Ce-1490 to 12 mol.% for CS-12Ce-1550, Figure 4 (a)). On CS-12Ce-1490 the diffusion depth was too small to be characterized by our EDS on cross sections. However, on CS-12Ce-1550 Ce was seen to diffuse up to 2 µm under the surface (Figure 4b), with a Ce/Zr molar ratio close to the surface around 10% (coherent with the surface observation) and an exponential decrease of the Ce concentration.

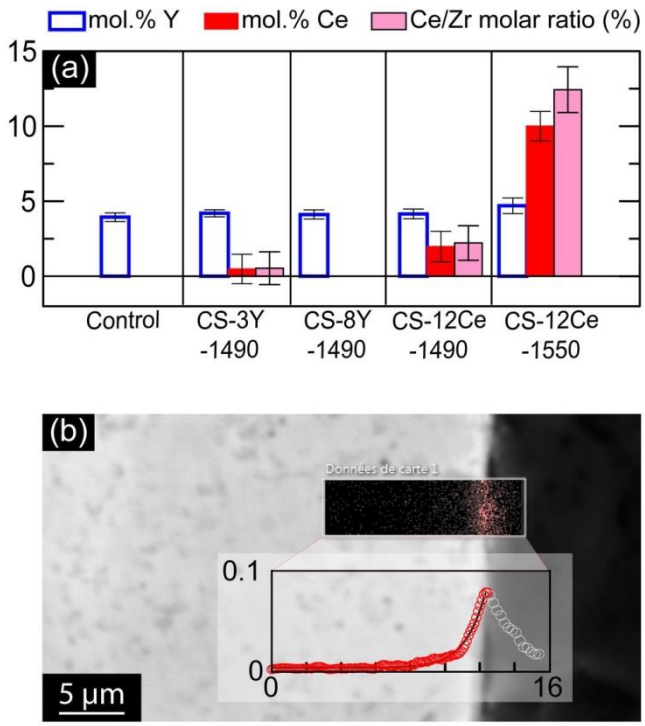

Figure 4: (a) EDS analyses on the surface of the different samples (Ce and Y molar fraction, Ce/Zr molar ratio); (b) example of cross sectional analysis of CS-12Ce-1550, with superimposed EDS map (intensity proportional to Ce molar fraction) and Ce/Zr molar ratio profile calculated from the map. The decreasing part of the profile is related to the probe size of the EDS analysis in the mounting resin around the sample, and has no meaning regarding the sample itself.

Table 2 : Composition analysis of CS samples: results are extracted from XRD data and Rietveld refinement unless specified otherwise.

Sample	wt.% c (XRD)	wt.% t (XRD)	wt.% Ce-t (XRD)	mol% Y_2O_3 in c (XRD)	mol% Y_2O_3 in t (XRD)	Grain size (nm)	Mol. % Y (EDS)	Mol. % Ce (EDS)
Precision	*± 0.5*	*± 0.5*	*± 0.5*	*± 0.05*	*± 0.05*	*± 10*	*≤ ±0.5*	*± 1*
Control*	25.9	52.3 + *21.7*	0	*NM*	*NM*	*NM*	3.9	0
Control + TT 1250°C	27.0	73.0	0	4.84	2.32	550	3.9	0
CS-3Y-1490	26.4	73.6	0	6.17	2.39	630	4.2	0.5
CS-8Y-1490	26.2	73.8	0	6.36	2.42	630	4.1	0
CS-12Ce-1490	33.5	66.5	0	*NM*	*NM*	1100	4.2	2.0
CS-12Ce-1550	33.1	65.2	1.7	*NM*	*NM*	2000	4.7	10

* *in the Control sample, machining procedure (performed by the producer) led to the apparition of shoulders on the left of diffraction peaks of the tetragonal phase, attributed to a "distorted tetragonal phase" accounting for 21.7 wt.% of the analysed material, and that prevented analysing the Y content in cubic and tetragonal phases, hence the second control treated at 1250°C to remove the distorted tetragonal phase. NM: not measurable (no calibration curve could be established)*

Mechanical properties

The crack propagation threshold and Vickers hardness of each group of sample are shown in Figure 5. Crack propagation thresholds (K_{I0}) fluctuate between 3.25 and 3.55 MPa.m$^{1/2}$. The control samples present a significantly higher propagation threshold. Among the treated

samples, only CS-12Ce-1490 presents a significantly lower K_{I0}, all the other ones present no significant differences among them (Table 3).

Vickers hardness was around 13.0 GPa, with no significant difference between treated samples (only Control sample was in some cases significantly harder, Table 4). Even though some statistically significant differences appeared, all these surface treatments allow retaining good mechanical properties.

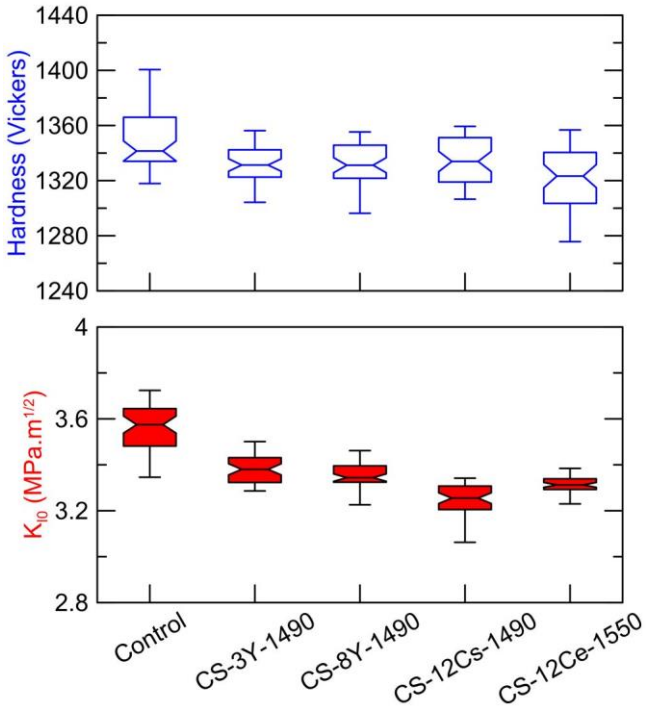

Figure 5 : Crack propagation threshold and Vickers hardness (notched box plot showing minimum and maximum (whiskers), median (notch) and lower and upper quartile (bottom and top of the box) for each series)

Table 3: statistical analysis of the K_{I0} results. K_{I0} are considered significantly different if P < 0.05 (ns P>0.05; * : 0.05>P>0.015; ** : 0.015>P>0.001; *** : 0.001>P>0.0001; *** : P<0.0001).

	Significant?	Summary	Adjusted P Value
Control *vs.* CS-3Y-1490	Yes	**	0.0071
Control *vs.* CS-8Y-1490	Yes	***	0.0003
Control *vs.* CS-12Ce-1490	Yes	****	<0.0001
Control *vs.* CS-12Ce-1550	Yes	****	<0.0001
CS-3Y-1490 *vs.* CS-8Y-1490	No	ns	>0.9999
CS-3Y-1490 *vs.* CS-12Ce-1490	Yes	***	0.0002
CS-3Y-1490 *vs.* CS-12Ce-1550	No	ns	0.4179
CS-8Y-1490 *vs.* CS-12Ce-1490	Yes	**	0.0063
CS-8Y-1490 *vs.* CS-12Ce-1550	No	ns	>0.9999
CS-12Cs-1490 *vs.* CS-12Ce-1550	No	ns	0.2866

Table 4: statistical analysis of the H_v results.

	Significant?	Summary	Adjusted P Value
Control *vs.* CS-3Y-1490	No	ns	0.0552
Control *vs.* CS-8Y-1490	Yes	*	0.0195
Control *vs.* CS-12Ce-1490	No	ns	0.1137
Control *vs.* CS-12Ce-1550	Yes	****	<0.0001
CS-3Y-1490 *vs.* CS-8Y-1490	No	ns	0.9953
CS-3Y-1490 *vs.* CS-12Ce-1490	No	ns	0.9982
CS-3Y-1490 *vs.* CS-12Ce-1550	No	ns	0.2892
CS-8Y-1490 *vs.* CS-12Ce-1490	No	ns	0.9591
CS-8Y-1490 *vs.* CS-12Ce-1550	No	ns	0.5108
CS-12Cs-1490 *vs.* CS-12Ce-1550	No	ns	0.1637

Analysis of ageing kinetics

The surface t-m phase transformation curves as a function of the hydrothermal ageing time are shown in Figure 6.The related parameters of ageing kinetics are summarized in Table 5. The thermal activation energies Q of CS-3Y-1490, CS-8Y-1490 and CS-12Ce-1490 are identical; around 110 kJ·mol^{-1}. However, CS-12Ce-1550 shows a strong resistance to ageing at 134°C, but ages faster than all other materials at 90°C, thus exhibits a lower activation energy (65 kJ·mol^{-1}). Figure 6 (f) shows the hydrothermal ageing kinetics measured at 134°C and extrapolated at 37°C for CS-3Y-1490 and CS-12Ce-1550 samples. Also the resistance to ageing of CS-12Ce-1550 samples at 134°C is the best of all samples (at 134°C it ages approximately 10 times slower than the other materials), it becomes the weakest of all at 37°C (ageing of CS-12Ce-1550 at 37°C is at least thrice faster as for other materials).

Table 5: Summary of the ageing parameters (from Eq. 3; V_0 was 0 for all materials). Q is given as Q_0 (Q_{min} – Q_{max}), were Q_0 is obtained from the data, and (Q_{min} – Q_{max}) gives an interval of confidence calculated supposing a 10% uncertainty on the monoclinic faction data

	V_{max}	n	b_0 (h^{-1})	Q (kJ/mol)
Control	0.8	1.55	$2.67 \cdot 10^{9}$	89.5 (89 – 95)
CS-3Y-1490	0.8	0.85	$6.62 \cdot 10^{12}$	112 (100 - 124)
CS-8Y-1490	0.8	0.82	$2.81 \cdot 10^{12}$	109 (98 - 121)
CS-12Ce-1490	0.68	1.48	$2.07 \cdot 10^{12}$	107 (100 - 117)
CS-12Ce-1550	0.62	2.23	$5.51 \cdot 10^{5}$	64.1 *(60 – 66)*

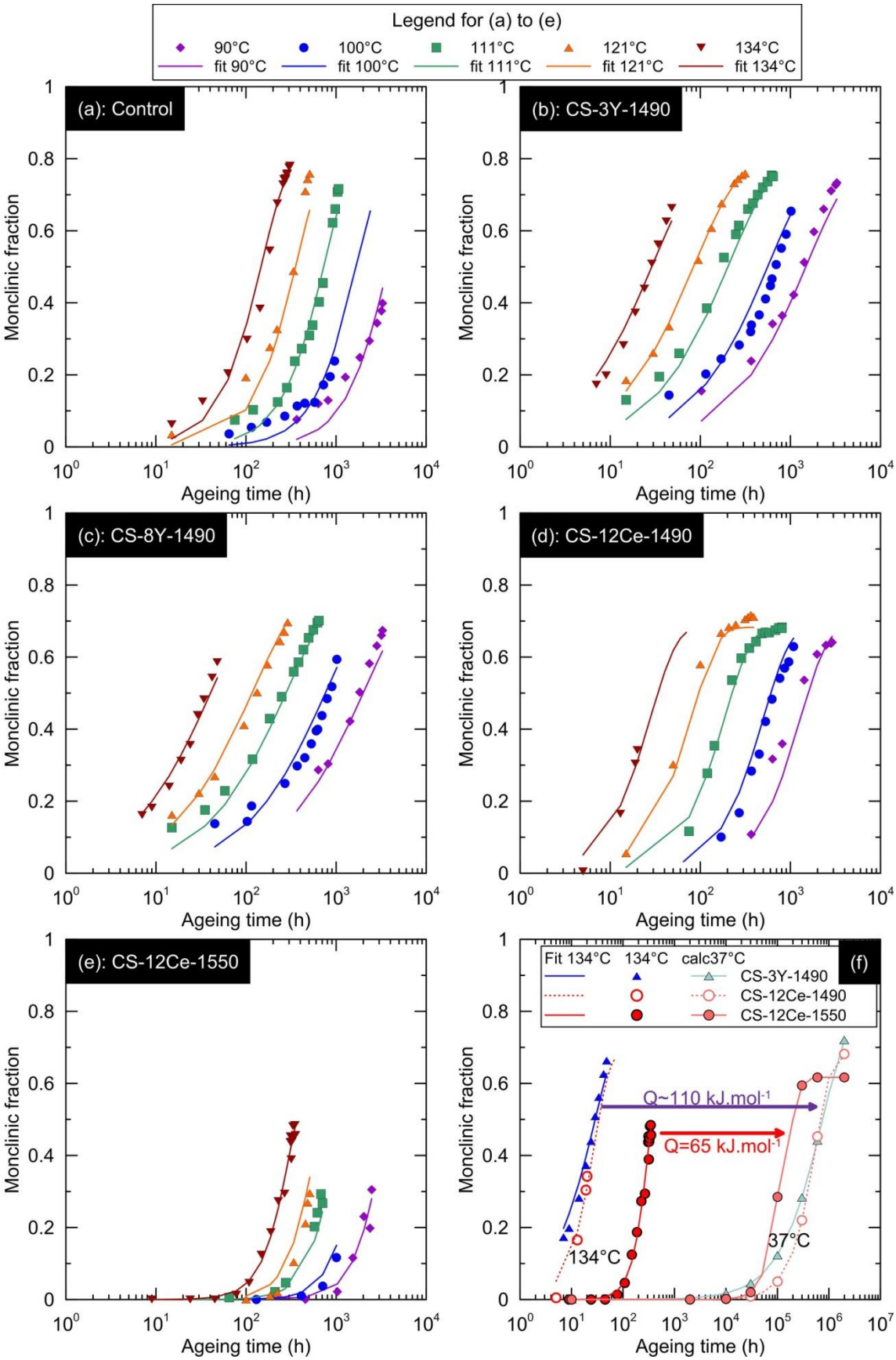

Figure 6: Hydrothermal ageing kinetics between 90 and 134°C for samples: (a) control, (b) CS-3Y-1490, (c) CS-8Y-1490, (d) CS-12Ce-1490, (e) CS-12Ce-1550. (f): Extrapolation of ageing kinetics to 37°C for CS-3Y-1490 and CS-12Ce-1550 samples, showing the influence of the different activation energies.

Discussions

The relationship between microstructure and doping with ceria and yttria

This work focuses on the change of the microstructure of zirconia samples placed on powders with different doping elements in post-sintering process. The results show that the grains on zirconia surfaces treated with 12Ce-TZP powder are growing more during the post-sintering treatment than the ones treated with Y-TZP powders, even though some large grains may appear in a small-grained matrix when treating with Y-stabilized zirconia. This is related to the segregation of yttrium at grain boundaries and the solute drag mechanism of dense zirconia grain growth at elevated temperature (>1200°C), which is highest for Y-TZP, and absent for Ce-TZP and moderate for Y, Ce-TZP [22-25].The results also show that more cubic phase appears on CS-12Ce samples. In the absence of external source of yttrium, the content of Y_2O_3 in the tetragonal phase should be reduced with the increase of the cubic phase content, accompanied by a large amount of yttrium into the cubic phase [26], in accordance with ZrO_2-Y_2O_3 phase diagram. However here the TZ8Y powder is an external Y source, thus small increases in Y content of both tetragonal and cubic phases take place in CS-8Y-1490 sample as measured by XRD. On the other hand, the overall Y enrichment remains small, undetectable by EDS (Table 2). Finally, coherently with diffusion mechanisms, more Ce is detected when the treatment is performed at high temperature.

Influence on mechanical properties

The results show small or negligible influence of surface treatments on H_V or K_{I0}. The control samples show significantly higher hardness and K_{I0}, probably due to machining surface residual stresses (shown by the distorted tetragonal phase, as can be seen on the XRD diagram on Figure 3 and on Table 2). All other materials were freed of these residual stresses during the thermal treatments on the powder beds.

Among other materials, the only significant difference found was a slightly lower K_{I0} for CS-12Ce-1490. On the other hand the K_{I0} was comparable for CS-12Ce-1550, CS-3Y-1490 and CS-8Y-1490.

Influence on ageing kinetic

Hydrothermal ageing should be considered in the light of the stabilization mechanisms of tetragonal zirconia phase. It is usually recognized that stabilisers of the t-phase in TZP materials can act through at least 2 mechanisms [1]: either by a steric effect (large ions, such as Ce^{4+}, that distort the cationic network), or by a vacancies effects (trivalent cations, such as Y^{3+} or Sc^{3+} that induce the formation of oxygen vacancies). During hydrothermal ageing, when oxygen vacancies get filled with water-derived species the tetragonal phase is destabilized (and the monoclinic one is over-stabilized) [27], which leads to the t-m transformation characteristic of zirconia ageing. Thus it is often considered that Y-TZP is sensitive to hydrothermal ageing due to the presence of oxygen vacancies, while Ce-TZP (with no or very few vacancies) is almost immune to it. Moreover, additional stabilization of Y-TZP by ceria has been proven to slow-down the ageing kinetics measured at high temperature (higher than 100°C) [28]. In addition, the hydrothermal ageing process occurs by a nucleation and growth mechanism [19], closely related to annihilation of oxygen vacancies [29-32]. Schubert and Frey [33] found that the penetration depth of water radicals during the ageing process is larger than the size of nucleus for martensitic transformations. The penetration of water radical leads to a lattice contraction, which leads to stress generation, and the stress accumulation is large enough to cause nucleation of the t-m transformation zone. For CS-12Ce-1550 samples, Ce ions are in solid solution in the zirconia lattice, on zirconium sites. Ce being tetravalent like zirconium, and since the amount of yttrium (trivalent) is not

changed, this does not result in a significant reduction in the number of oxygen vacancies on the sample surface. The delayed ageing at 134 °C may thus be explained by a combination of the stabilizing effects of Y (oxygen vacancy plus size effect) and Ce (size effect), and a globally higher stability of tetragonal phase (at 134°C).

As the ageing process of Ce-TZP at 134°C is very slow, activation energy for ageing of Ce-TZP and Ce-Y-TZP are seldom, if ever, reported. Our results show that the activation energy for ageing of Y-Ce-tetragonal zirconia can be lower than the one of Y-TZP (~65 $kJ \cdot mol^{-1}$ measured for CS-12Ce-1550, vs ~100 $kJ \cdot mol^{-1}$ for all other materials; the estimation of the interval of confidence shown in Table 5 show that this difference is significant). As a result, Y-Ce-tetragonal phase (in CS-12Ce-1550) exhibits a strong resistance to ageing at 134°C, similarly to what was observed for instance by Marro et al. [28]. But it exhibits the lowest resistance to ageing at 37°C of all the materials tested here. For CS-12Ce-1490 samples, the activation energy is not reduced.

Since activation energy is very long to measure (sometimes several thousand hours of experiments), only limited data are available in the literature. Among these limited data, to our knowledge low activation energies (much lower than the usual ~100kJ/mol) were observed in 4 different cases:

- In Wei et al.[10], material PS1150-200h: long thermal treatment at low temperature, intermediate grain size (0.3 µm), rather low fraction of Y in the tetragonal phase and high Y fraction in the cubic phase (Q=41 kJ/mol)
- In Gremillard et al.[34] in a zirconia toughened alumina material (20% zirconia) (Q=50 kJ/mol)
- In Deville et al.[35], in a zirconia-toughened alumina (17vol. % 3Y-TZP, grain size: 1.2 µm for alumina, 0.5 µm for zirconia) (Q=78 kJ/mol); here the low activation energy was attributed to the fact that in this material only nucleation of the t-m transformation occurs during ageing (there is no growth stage).
- Here : high temperature treatment in the presence of Ce-TZP, leading to grain growth and high amount of Ceria in the surface layers of the material

A priori the common features among these 4 materials are not obvious.
It is believed, without definitive proof however, that the activation energy may be linked to a few different parameters:

- Activation energy of water diffusion in zirconia, that may change with the crystal structure (dopants, oxygen vacancies… for diffusion through the grains) and with the grain boundaries structure (dopants, glass phase… for diffusion through the grain boundaries)
- Presence of residual stresses
- Acceleration of oxygen vacancies diffusion, in the presence of a source or a trap of vacancies.

In view of these hypotheses, the slightly lower activation energy of control material might be related to the presence of residual stresses. However the much lower activation energy of CS-12Ce-1550 cannot be related to residual stresses (the material was thermally treated). Thus only few hypotheses remain to explain it:

1- the lattice distortions induced by the presence of a large amount of Ce ions in the structure (on the surface of the material at least) may change the activation energy of water diffusion
2- the higher treatment temperature may have triggered a reduction of Ce (ions from Ce+IV to Ce+III), generally followed by a migration of Ce^{3+} ions to the grain

boundaries, and here the phase transformation during ageing might be controlled by complex diffusion of oxygen vacancies from the grain boundaries to the grains (in the zone containing Cerium), and between the bulk (Ce-free) and the surface (Ce-rich), with an activation energy different from the activation energy of water diffusion.

We have to acknowledge that this discussion is highly speculative. Its main purpose is thus to provide hypotheses for further exploration.

Conclusions

This article introduced a method to delay ageing at high temperature: doping the surface of 3Y-TZP samples with cerium (the source of cerium being 12Ce-TZP powder). The most efficient treatment (30 min at 1550°C) results in a ~10%Ce-doping over less than 2µm depth. Ageing at 134°C can be delayed by this treatment, while hardness and crack propagation threshold are mostly preserved. However, the activation energy of ageing is decreased, and that impacts negatively the resistance to ageing at lower temperature. This highlights the need, for ever new zirconia-based material, to quantify ageing not only at 134°C, but also at other temperatures so that the ageing behaviour can be extrapolated at use temperature, in order to avoid potentially severe underestimation of ageing kinetics at use temperature in spite of good ageing resistance at test temperature (134°C).

Acknowledgments

C. Wei was supported by a grant from the Chinese Scholarship Council.

The authors wish to acknowledge Dr. Sandrine Dankic-Cottrino for her help with granulometry measurements.

References

[1] J. Chevalier, L. Gremillard, D.R. Clarke, A.V. Virkar, The tetragonal-monoclinic transformation in zirconia: Lessons learned and future trends, Journal of the American Ceramic Society 92 (9) (2009) 1901-1920

[2] S. Lawson, Environmental degrdation of zirconia ceramics, Journal of the european ceramic society 15 (1995) 485-502

[3] E. Lilley, Environmental degradation in Y-TZPs, In: Corrosion and corrosive degradation of ceramics,Ceramic transactions 10 (1990)

[4] J. Chevalier, L. Gremillard, S. Deville, Low temperature degradation of zirconia and its implication on biomedical implants, Annual Review of Materials Research 37 (2007) 1-32.

[5] J. Chevalier, J. Loh, L. Gremillard, S. Meille, E. Adolfson, Low-temperature degradation in zirconia with a porous surface, Acta Biomaterialia 7(7) (2011) 2986-2993.

[6] C. Oblak, I. Verdenik, M.V. Swain, T. Kosmac, Survival-rate analysis of surface treated dental zirconia (Y-TZP) ceramics, Journal of Materials Science: Materials in Medicine 25(10) (2014) 2255-2264.

[7] S. Deville, J. Chevalier, L. Gremillard, Influence of surface finish and residual stresses on the ageing sensitivity of biomedical grade zirconia, Biomaterials 27(10) (2006) 2186-2192.

[8] M. Inokoshi, K. Vanmeensel, F. Zhang, J. De Munck, G. Eliades, S. Minakuchi, I. Naert, B. Van Meerbeek, J. Vleugels, Aging resistance of surface-treated dental zirconia, Dental Materials 31(2) (2015) 182-194.

[9] E. Camposilvan, F.G. Marro, A. Mestra, M. Anglada, Enhanced reliability of yttria-stabilized zirconia for dental applications, Acta Biomaterialia 17 (2015) 36-46.

[10] C. Wei, L. Gremillard, Towards the prediction of hydrothermal ageing of 3Y-TZP bioceramics from processing parameters, Acta Materialia 144 (2018) 245-256.
[11] F. Lange, D. Marshall, J. Porter, Controlling Microstructures Through Phase Partitioning from Metastable Precursors The ZrO2–Y2O3 System, Ultrastructure processing of advanced ceramics (1988) 519-532.
[12] H.G. Scott, Phase relationships in the zirconia-yttria system, Journal of Materials Science 10(9) (1975) 1527-1535.
[13] T. Stoto, M. Nauer, C. Carry, Influence of Residual Impurities on Phase Partitiioning and Grain Growth Processes of Y-TZP Materials, Journal of the American Ceramic Society 74(10) (1991) 2615-2621.
[14] G. Anstis, P. Chantikul, B.R. Lawn, D. Marshall, A critical evaluation of indentation techniques for measuring fracture toughness: I, direct crack measurements, Journal of the American Ceramic Society 64(9) (1981) 533-538.
[15] N. Garmendia, S. Grandjean, J. Chevalier, L.A. Diaz, R. Torrecillas, I. Obieta, Zirconia-multiwall carbon nanotubes dense nano-composites with an unusual balance between crack and ageing resistance, Journal of the European Ceramic Society 31[6] (2011) 1009-14.
[16] C. Olagnon, J. Chevalier, V. Pauchard, Global description of crack propagation in ceramics, Journal of the European Ceramic Society 26[15] (2006) 3051-59.
[17] H. Toraya, M. Yoshimura, S. Somiya, Calibration Curve for Quantitative Analysis of the Monoclinic-Tetragonal ZrO2 System by X-Ray Diffraction, Journal of the American Ceramic Society 67(6) (1984).
[18] R.C. Garvie, P.S. Nicholson, Phase analysis in zirconia systems, Journal of the American Ceramic Society 55(6) (1972) 303-305.
[19] J. Chevalier, B. Cales, J.M. Drouin, Low-Temperature Aging of Y-TZP Ceramics, Journal of the American Ceramic Society 82(8) (1999) 2150-2154.
[20] L. Gremillard, J. Chevalier, T. Epicier, S. Deville, G. Fantozzi, Modeling the aging kinetics of zirconia ceramics, Journal of the European Ceramic Society 24(13) (2004) 3483-3489.
[21] T.E. Everhart, P.H. Hoff, Determination of kilovolt electron energy dissipation vs penetration distance in solid materials. Journal of Applied Physics 42(13) (1971) 5837:5846..
[22] M.M.R. Boutz, A.J.A. Winnubst, A.J. Burggraaf, Yttria-ceria stabilized tetragonal zirconia polycrystals: Sintering, grain growth and grain boundary segregation, Journal of the European Ceramic Society 13(2) (1994) 89-102.
[23] G.S.A.M. Theunissen, A.J.A. Winnubst, A.J. Burggraaf, Effect of dopants on the sintering behaviour and stability of tetragonal zirconia ceramics, Journal of the European Ceramic Society 9(4) (1992) 251-263.
[24] G.S.A.M. Theunissen, A.J.A. Winnubst, A.J. Burggraaf, Surface and grain boundary analysis of doped zirconia ceramics studied by AES and XPS, Journal of Materials Science 27(18) (1992) 5057-5066.
[25] S.-L. Hwang, I.W. Chen, Grain Size Control of Tetragonal Zirconia Polycrystals Using the Space Charge Concept, Journal of the American Ceramic Society 73(11) (1990) 3269-3277.
[26] J. Chevalier, S. Deville, E. Münch, R. Jullian, F. Lair, Critical effect of cubic phase on aging in 3mol% yttria-stabilized zirconia ceramics for hip replacement prosthesis, Biomaterials 25(24) (2004) 5539-5545.
[27] A.G. Gebresilassie, Atomic scale simulations in zirconia : Effect of yttria doping and environment on stability of phases. PhD thesis, INSA-Lyon (2016). http://theses.insa-lyon.fr/publication/2016LYSEI038/these.pdf
[28] F. Marro, J. Valle, A. Mestra, M. Anglada, Surface modification of 3Y-TZP with cerium oxide, Journal of the European Ceramic Society 31(3) (2011) 331-338.

[29] X. Guo, Hydrothermal degradation mechanism of tetragonal zirconia, Journal of materials science 36(15) (2001) 3737-3744.
[30] X. Guo, Property Degradation of Tetragonal Zirconia Induced by Low-Temperature Defect Reaction with Water Molecules, Chemistry of Materials 16(21) (2004) 3988-3994.
[31] G. Pezzotti, M.C. Munisso, A.A. Porporati, K. Lessnau, On the role of oxygen vacancies and lattice strain in the tetragonal to monoclinic transformation in alumina/zirconia composites and improved environmental stability, Biomaterials 31(27) (2010) 6901-6908.
[32] F. Zhang, M. Batuk, J. Hadermann, G. Manfredi, A. Mariën, K. Vanmeensel, M. Inokoshi, B. Van Meerbeek, I. Naert, J. Vleugels, Effect of cation dopant radius on the hydrothermal stability of tetragonal zirconia: Grain boundary segregation and oxygen vacancy annihilation, Acta Materialia 106 (2016) 48-58.
[33] H. Schubert, F. Frey, Stability of Y-TZP during hydrothermal treatment: neutron experiments and stability considerations, Journal of the European Ceramic Society 25(9) (2005) 1597-1602.
[34] L. Gremillard, J. Chevalier, L. Martin, T. Douillard, S. Begand, K. Hans, T. Oberbach, Sub-surface assessment of hydrothermal ageing in zirconia-containing femoral heads for hip joint applications, Acta Biomaterialia 68 (2018) 286-95.
[35] S. Deville, J. Chevalier, C. Dauvergne, G. Fantozzi, J.F. Bartolomé, J.S. Moya, R. Torrecillas, Microstructural investigation of the aging behavior of (3Y-TZP)-Al_2O_3 composites, J. Am. Ceram. Soc. 88[5] (2005) 1273-80.